



RESEARCH MEMORANDUM

EFFECT OF WING SIZE AND AMOUNT OF INDENTATION ON
APPLICABILITY OF TRANSONIC AREA RULE TO
SWEPT-WING CONFIGURATIONS

By James Rudyard Hall

Langley Aeronautical Laboratory
Langley Field, Va.

NATIONAL ADVISORY COMMITTEE
FOR AERONAUTICS
WASHINGTON

July 20, 1956
Declassified December 4, 1957

NATIONAL ADVISORY COMMITTEE FOR AERONAUTICS

RESEARCH MEMORANDUM

EFFECT OF WING SIZE AND AMOUNT OF INDENTATION ON
APPLICABILITY OF TRANSONIC AREA RULE TO
SWEPT-WING CONFIGURATIONS

By James Rudyard Hall

SUMMARY

A systematic transonic zero-lift drag investigation utilizing a swept-wing configuration having three different ratios of wing to fuselage size has been conducted at the Langley Pilotless Aircraft Research Station at Wallops Island, Va., utilizing the 6-inch helium gun. The experiments and comparisons with results of other swept-wing configurations indicated that the reduction of pressure drag obtainable from partial indentation is approximately proportional to the amount of indentation employed up to a Mach number of 1.3. The extent to which an equivalent body approximates the drag of its parent wing-body configuration depends upon the wing size, agreement being better for smaller wings. Generally, for unindented swept-wing configurations it is possible to obtain the pressure drag within 10 percent up to about Mach number 1.2 by dividing the pressure drag of the equivalent body of a swept-wing configuration by the ratio of the pressure-drag coefficient for the equivalent body to the pressure-drag coefficient for the configuration obtained from the present tests.

In two cases it has been possible to approximate the pressure drag of a swept-wing configuration with an equivalent body incorporating an average wing projection. The agreement was within 10 percent below Mach number 1.17 with the best agreement being obtained near a Mach number of 1.0. Wing-fuselage interference drag did not vary appreciably for the three wing sizes tested for unindented bodies.

INTRODUCTION

Since the transonic area rule first came into prominence with reference 1, it has been the subject of considerable research effort (for example, refs. 2 to 12). Specifically, reference 1 defined the rule as

follows: ". . . near the speed of sound the zero-lift drag-rise of a thin low-aspect-ratio wing-body combination is primarily dependent on the axial distribution of cross-sectional areas normal to the air stream." This can be applied in two ways: (1) reduction of aircraft pressure drag by arrangement of components to give good area distribution, including indenting the fuselage to relieve all or part of the cross-sectional-area concentrations due to the components and (2) approximation of the pressure drag of an aircraft configuration by its equivalent body of revolution. The rule has been found to apply very well to the first of these applications, particularly for swept-wing configurations where the rate of growth of wing cross-sectional area is low and indentations are gradual and comparatively shallow. The second application has been found to yield approximations within 15 percent for delta and unswept wings. A semiempirical study made by the Consolidated Vultee Aircraft Corporation on the range of applicability of the transonic area rule to 70 configurations lead to a conclusion that direct correlation separated for values of the parameter $A(t/c)^{1/3}$ greater than unity. This same parameter has been shown by Spreiter in reference 13 to be the boundary for correlation of the drag rise for families of rectangular wings. The current investigation was undertaken to obtain information of a systematic nature on the area rule in the region where $A(t/c)^{1/3}$ was greater than unity. Wing scale effects, indentations, and equivalent bodies of revolution were to be investigated, utilizing a swept wing with $A(t/c)^{1/3} = 1.57$. The program consisted of a zero-lift drag study of a swept-wing configuration having three different ratios of wing to fuselage size. Flight tests were made of the basic fuselage, the basic fuselage plus wing configurations and their equivalent bodies of revolution, indented fuselage plus wing configurations and their equivalent bodies of revolution, and bodies of revolution incorporating special methods of projecting the wing area onto the fuselage. It is to be noted that, since the thickness ratio enters only to the $1/3$ power, the parameter is relatively less sensitive to variations of thickness than aspect ratio. Contemporary swept-wing airplane configurations with aspect ratios from 4 to 3 and thickness ratios from 0.10 to 0.06 have corresponding values of $A(t/c)^{1/3}$ from 1.86 to 1.17.

SYMBOLS

A aspect ratio

C_D drag coefficient, Drag/qS_F

ΔC_D pressure-drag coefficient, $C_D - C_{D\text{subsonic}}$

K	ratio of $\frac{\text{EBR } \Delta C_D}{\text{Config } \Delta C_D}$ for the present configuration to $\frac{\text{EBR } \Delta C_D}{\text{Config } \Delta C_D}$ for an airplane configuration of appropriate wing-fuselage size ratio
<i>l</i>	overall length of fuselage, in.
M	Mach number
R	radius of fuselage, in.
S	cross-sectional area, sq in.
S_W	maximum wing cross-sectional area, sq in.
S_F	fuselage frontal area, sq in.
S_p	plan-form area of wing, sq in.
t/c	ratio of thickness to chord
X	fuselage station, in.

Subscripts:

W	refers to wing plus interference
I	refers to indented fuselage
U	refers to unindented fuselage
max	maximum

In this paper, the equivalent body of revolution is designated EBR; the configuration is designated Config.

EXPERIMENTAL VEHICLES

The basic configurations used in these experiments are shown in figure 1 along with pertinent physical dimensions. Three ratios of wing to fuselage size were used, the ratios of wing plan-form area to fuselage frontal area being 15.97, 11.80, and 8.90. The corresponding ratios of maximum cross-sectional wing area to fuselage frontal area

were 0.490, 0.360, and 0.277. Hereinafter the configurations with these dimensions will be called the large, medium, and small winged configurations, respectively. The variation of wing-fuselage size ratio was obtained by the use of two wing sizes and two fuselage sizes, the linear scale of the smaller wing and fuselage being seven-eighths of the larger. These components were combined in the following manner: (1) large wing on small fuselage (called large wing configuration), (2) large wing on large fuselage (called medium wing configuration), and (3) small wing on large fuselage (called small wing configuration). The basic fuselage is composed of a pointed parabolic forebody of fineness ratio 5.75, a cylindrical center section of fineness ratio 2.50, and a parabolic afterbody of fineness ratio 4.75 with a ratio of base to maximum diameter of 0.4. This high-fineness-ratio fuselage is characterized by very low base drag. Unpublished measurements show that the supersonic base drag coefficient for a very similar configuration is 0.013 (based on frontal area) and the subsonic base drag coefficient is about 0.009. For purposes of obtaining pressure drag, the base drag will be assumed constant. The coordinates of the basic fuselage are given in table I. The wing described in figure 1 utilizes an NACA 65A006 airfoil section in the free-stream direction and has an aspect ratio of 4, a taper ratio of 0.3, and a 45° sweep of the 1/4-chord line.

From the basic wingless configuration and the three basic winged configurations, the following vehicles were derived and tested:

- (a) Equivalent body of large, medium (model failed), and small wing configurations.
- (b) Large, medium, and small wing configurations with the body indented to compensate for the normal cross-sectional area of the exposed wing.
- (c) Large and medium wing configurations with the body indented to compensate for half the normal cross-sectional area of the exposed wing.
- (d) Equivalent bodies of the two test vehicles in (c).
- (e) Equivalent body of medium wing configuration with the wing cross-sectional area taken along slices parallel to the wing maximum-thickness line (40 percent chord). This equivalent body is hereinafter referred to as having the root wing projection.
- (f) Equivalent body of medium wing configuration with the wing cross-sectional area taken as the average between that described in (e) and the normal cross-sectional slices. This equivalent body is herein-after referred to as having the average wing projection.

Note that the wingless configuration serves as the equivalent body of revolution of the fully indented configurations.

In table II the program is tabulated in related groups for quick reference. Photographs of the test vehicles are presented in figure 2. Nondimensional area distributions of the test vehicles are given in figure 3.

The test vehicles were constructed of 2024 (24S) aluminum alloy except for brass noses. The center of gravity of the test vehicles varied between 43 and 48 percent of the body length from the nose. In terms of the mean aerodynamic chord, the most rearward center-of-gravity location was at -10 percent of the mean aerodynamic chord.

EXPERIMENTAL TECHNIQUE

The experiments were conducted at the Langley Pilotless Aircraft Research Station at Wallops Island, Va., utilizing the 6-inch helium gun. The operation of this facility and the method of obtaining drag coefficients is described in reference 12. Briefly, the 6-inch helium gun operates by propelling the test vehicle to supersonic velocities by means of compressed helium, whereupon the model is tracked by a Doppler velocimeter giving a velocity history of the flight. The flight path is assumed to be a ballistic trajectory for these zero-lift test vehicles. Atmospheric conditions are determined by means of radiosonde and wind-sonde measurements.

The Reynolds numbers of the tests, based on the length of the test vehicles, varied between 8.7×10^6 at Mach number 1.4 and 3.9×10^6 at Mach number 0.8.

The accuracy of the measured quantities due to instrument and reduction limitations lies within the following limits:

The measured quantities were used to derive ratios presented later in the report. Calculation of these ratios involved subtracting coefficients of similar magnitude which resulted in the following possible inaccuracies for three Mach numbers:

	M	Possible inaccuracy
$\frac{(\Delta C_{DW})_{\text{fully indented}}}{(\Delta C_{DW})_{\text{unindented}}}$	1.05	0.05
	1.20	.08
	1.40	.10
$\frac{(\Delta C_{DW})_{1/2 \text{ indented}}}{(\Delta C_{DW})_{\text{unindented}}}$	1.05	.07
	1.20	.10
	1.40	.12
<u>Equiv body ΔC_D</u>	1.05	.04
	1.20	.04
	1.40	.04

RESULTS AND DISCUSSION

Basic Data

Figures 4 to 9 present the measured drag coefficients and the drag-rise coefficients for the test vehicles in related groups, namely, the wingless configuration (fig. 4), the basic fuselage plus wing configurations (fig. 4), the equivalent bodies of the wing-body configurations (fig. 5), the wing-body configurations with the body fully indented for the wing cross-sectional area (fig. 6), the wing-body configurations with the body indented to compensate for half the wing cross-sectional area (fig. 7), equivalent bodies of the configurations in figure 7 (fig. 8), and special wing projections (fig. 9). The Reynolds number of the experiments based on the large fuselage length was 8.7×10^6 at Mach number 1.4 and decreased to 3.9×10^6 as the vehicles decelerated to Mach number 0.8. The Reynolds numbers based on the mean aerodynamic chord of the large wing and tail at Mach number 1.4 were 1.2×10^6 and 0.6×10^6 , respectively.

Total Drag

The small scale and the aerodynamically clean lines of the vehicles used in these experiments raise the question of the type of flow prevailing during the flight. Comparison of the measured subsonic drag levels with the skin-friction theory of Van Driest (ref. 14) reveals that for some of the results, variations of subsonic level exist above those predicted by Van Driest theory when turbulent flow is assumed to exist over all except the nose of the vehicle. The magnitude of the experimental departure from this theoretical level is approximately the

same in every case in which departure occurs (difference in subsonic $C_D = 0.030$). The magnitude of the difference can be accounted for by assuming turbulent flow instead of laminar flow over the nose. Although many other combinations of changes in flow from a given state to a more turbulent state can be assigned to explain the differences observed in subsonic C_D , the important thing is that the differences were constant for every case in which departure from the initially assumed condition occurred. The assumption that the change in flow over the nose can account for the sometimes observed difference in subsonic C_D merely helps visualize the extent of the surface affected. Assuming that one of two flow states existed on the test vehicles at subsonic velocities, and designating the fully turbulent C_D level as high and the partly turbulent C_D level as low (symbols at $M = 0.85$ represent the theoretical partly turbulent level), a comparison of the experimental curves and corresponding symbols in figures 4 to 9 shows the following: The medium wing configuration exhibits the lower subsonic C_D , whereas the large and small wing configurations have the higher C_D ; the equivalent bodies of the winged configurations have the higher subsonic C_D , whereas the fully indented winged configurations have the lower C_D ; the half-indented large winged configuration and its equivalent body of revolution have the lower C_D , whereas the corresponding medium wing vehicles have the higher C_D ; and, finally, both special wing projections have the higher subsonic level. The fact that the presence or absence of the wing had no systematic effect on the subsonic level suggests that any change in transition had a negligible effect on the drag of afterbody, fins, and wings.

The drag curve for the wingless configurations shows a sudden drop between Mach numbers 1.07 and 1.05 for the decelerating model of the same magnitude that exists between the subsonic level of the drag coefficients. This is probably a transition phenomenon and shows how rapidly transition can occur and verifies the magnitude of the change involved. Since the phenomenon is not evidenced in any of the other drag curves, it is probable that it occurred during the drag rise in these cases.

Subsequently, it will be assumed that the flow was entirely turbulent at supersonic speeds for all the test flights and that it remained turbulent through the transonic drag rise for some flights; for others, transition occurred over the nose as the model decelerated to subsonic velocities through the transonic drag rise. For purposes of calculation, all the drag curves will be adjusted to the condition corresponding to the partly turbulent state at subsonic speeds. The curves of total-drag coefficient (figs. 4 to 9) to which adjustments must be made are marked with an asterisk and have the adjusted subsonic levels shown by means of the symbols located at Mach number 0.85. The change in pressure-drag coefficients effected by these adjustments is shown also by means of

symbols for a range of Mach number for the large and small winged configurations (fig. 4) as typical of all the models in which adjustments are required. The medium winged configuration had partly turbulent subsonic flow and required no adjustment. All results presented which are affected by this assumption will be shown by a heavy bar connected to the symbol to show the magnitude of the change which would occur had the assumption not been made.

Pressure Drag

Figure 10 compares, for several Mach numbers, the wing-plus-interference pressure-drag reduction attained with different amounts of fuselage indentation. The wing pressure drag was taken as the difference between the pressure drag of the winged configuration and that of the basic unindented wingless configuration. The quantity was determined for the fully indented and half-indented configurations. It is seen that, for low supersonic Mach numbers, the wing pressure drag can be virtually eliminated by full indentation and that half indentation achieves about a 50 percent reduction of wing pressure drag. As the Mach number increases, the reductions begin to diminish, although the variation with amount of indentation at particular Mach numbers remains approximately linear. This result is in keeping with experience regarding the drag of an indented wing-body combination at Mach numbers beyond the design point and with the results of references 10 and 11 and the extrapolated results of references 1 and 15, wherein normal indentation required to relieve the wing, although effectual in reducing drag in the transonic region, produced unfavorable increases beyond this range. The increased drag of the indented configuration must be associated with greater interference and/or suction on the forward face of the indentation, as well as with the decreasing effectiveness of the indentation as the Mach number increases. Even allowing for the possible variation due to inherent inaccuracies, the results establish a trend and indicate that, for swept-wing configurations, some advantage of indentation may be obtained up to Mach number 1.3 by partial indentation with the sacrifice of additional pressure drag at the lower supersonic Mach numbers.

The wing-plus-interference drag coefficients of the unindented configurations (obtained by subtracting the drag coefficient of the wingless configuration from that of the winged configuration) based on the wing area are the same for all three wing sizes within the measurement accuracies quoted, indicating that interference drag does not vary appreciably with wing size.

Equivalent Bodies

The equivalent bodies of swept-wing configurations have consistently given much lower pressure drag than that experienced by the actual configurations. An explanation of this phenomenon advanced in reference 12 is that, in the equivalent body of revolution, the wing area distribution is projected normally onto the fuselage, whereas for the configuration the region of wing-fuselage pressure interaction is concentrated in the region of the wing root, leading to a lower effective equivalent-body fineness ratio and a higher pressure drag for the configuration. The current investigation permits an evaluation of the effect of wing size on this phenomenon. The drag rise of the equivalent bodies of the subject configurations has been summarized in figure 11 by plotting the fraction of equivalent-body pressure drag to configuration pressure drag against wing-fuselage size ratio (S_w/S_f) for various Mach numbers. The experimental points were joined and faired to zero wing ratio for each Mach number, inasmuch as the configuration pressure drag must equal the equivalent-body pressure drag when the wing becomes vanishingly small. The measured drag of corresponding equivalent bodies and configurations exhibited the same type of subsonic flow in every case; hence, the accuracy of these comparisons is limited only by the measurement accuracies quoted previously. The figure shows that, for unindented configurations, the wing size bears a direct relationship to how closely the configuration pressure drag may be duplicated by the equivalent body of revolution. As might be expected, closer agreement is obtained with smaller wings. The agreement falls off rapidly with increasing Mach number. The curves for the fully indented configuration indicate that much closer agreement of equivalent-body and configuration pressure drag may be expected at low supersonic Mach numbers and for small winged configurations. The half-indented configurations indicate an unexplained change of slope which is arbitrarily faired to the zero point in order to determine values of the ordinate which will be used in figure 12.

The values of $\frac{EBR \Delta C_D}{Config \Delta C_D}$ given in figure 11 are compared in figure 12 for the same size ratio measured for a number of swept-wing airplane and research configurations (refs. 10, 11, 12, 16, and 17) to determine the suitability of this parameter as a means of correlating the measured equivalent-body pressure drag with configuration pressure drag.

The comparison is made in the form of a ratio K of $\frac{EBR \Delta C_D}{Config \Delta C_D}$ determined by the current experiments to $\frac{EBR \Delta C_D}{Config \Delta C_D}$ measured for the

airplane configurations in the referenced experiments. The value 1.0 corresponds to perfect agreement between the presented results and those of the references and means that the values of $\frac{EBR \Delta C_D}{Config \Delta C_D}$ measured

herein can be applied generally to swept-wing configurations to correct the pressure drag measured for an equivalent body of revolution to the true values of pressure drag for the parent airplane configuration. For Mach numbers below 1.3, the unindented configurations with low ratios of base to frontal area (given in fig. 12) fall within 10 percent of the line of perfect agreement. The configurations with the larger bases or blunter afterbodies show poor correlation. However, when base-pressure measurements were used to eliminate the base drag from the drag of configuration C, excellent correlation resulted as shown by configuration C'. Although no base-pressure measurements were available for the other large base models, estimates of the base drag corrections for model E indicate that an improved correlation would result. Two conclusions may be drawn from these data: (1) For unindented swept-wing configurations it is possible to determine ΔC_D within 10 percent up to Mach number 1.3 by

dividing the pressure drag of the equivalent body by the ratio $\frac{\text{EBR } \Delta C_D}{\text{Config } \Delta C_D}$

as determined from the present tests; (2) for models with large ratios of base to frontal area, it is apparently incorrect to assume that the base pressure drag is the same for the equivalent body of revolution and the parent configuration.

Special Projections

The explanation advanced previously as to why the pressure drag of equivalent bodies of swept-wing configurations was consistently lower than the pressure drag of the configuration was explored with two test vehicles, wherein the wing area was projected onto the fuselage in different fashions (described in the section on experimental vehicles). The drag curves of these vehicles are shown in figure 9. The subsonic level of these curves indicates that the subsonic flow was turbulent. In order to compare the curves with their corresponding configuration, the subsonic levels were adjusted to the laminar level as previously described. Comparison of the equivalent bodies and the configuration is made in figure 13 by plotting the ratio $\frac{\text{EBR } \Delta C_D}{\text{Config } \Delta C_D}$ against Mach number. The experi-

mental points are again shown with symbols connected to heavy bars to indicate the magnitude of the change which would occur if the subsonic level of the equivalent bodies had not been shifted. It can be seen that the root wing projection gives values of the ratio $\frac{\text{EBR } \Delta C_D}{\text{Config } \Delta C_D}$ of about 2,

indicating that such a wing projection gives too severe an area concentration to approximate the configuration drag. The average wing projection gives agreement within 10 percent throughout the Mach number range. If the subsonic drag of the equivalent bodies had not been adjusted to the laminar level, the above comparisons would not have changed appreciably, especially at the lower Mach numbers. Shown in figure 13 are

the results of unpublished experiments with a swept wing configuration incorporating an average wing projection in which the same type of comparative drag rise was obtained. The latter two cases indicate that it may be possible to approximate the pressure drag of a swept-wing configuration with an equivalent body incorporating an average wing projection. If so the experiments show that the approximation is best made close to a Mach number of 1.0.

CONCLUSIONS

The results of an investigation to explore the range of applicability of the transonic area rule to swept-wing configurations indicates the following conclusions:

1. The reduction in pressure drag obtainable from partial indentation is approximately proportional to the amount of indentation employed up to a Mach number of 1.3.
2. The extent to which the drag of an equivalent body approximates the drag of its parent wing-body configuration depends upon the wing size, agreement being better for smaller wings for the unindented and fully indented configurations. Generally, for unindented swept-wing configurations it is possible to obtain the pressure drag within 10 percent up to about Mach number 1.2 by applying the ratio of the pressure-drag coefficient of the equivalent body to the pressure-drag coefficient of the configuration as measured for the present configuration to the measured pressure drag of the equivalent body of the configuration.
3. In two cases it was possible to approximate the drag of a swept wing configuration with an equivalent body incorporating an average wing projection. The agreement was best close to a Mach number of 1.0 and diverged to 10 percent at Mach number 1.17.
4. The wing-fuselage interference drag coefficient did not vary appreciably for the three wing sizes tested for unindented bodies.

Langley Aeronautical Laboratory,
National Advisory Committee for Aeronautics,
Langley Field, Va., June 6, 1955.

REFERENCES

1. Whitcomb, Richard T.: A Study of the Zero-Lift Drag-Rise Characteristics of Wing-Body Combinations Near the Speed of Sound. NACA RM L52H08, 1952.
2. Loving, Donald L.: A Transonic Wind-Tunnel Investigation of the Effect of Modifications to an Indented Body in Combination With a 45° Sweptback Wing. NACA RM L53F02, 1953.
3. Robinson, Harold L.: A Transonic Wind-Tunnel Investigation of the Effects of Body Indentation, As Specified by the Transonic Drag-Rise Rule, on the Aerodynamic Characteristics and Flow Phenomena of a 45° Sweptback-Wing—Body Combination. NACA RM L52L12, 1953.
4. Williams, Claude V.: A Transonic Wind-Tunnel Investigation of the Effects of Body Indentation, As Specified by the Transonic Drag-Rise Rule, on the Aerodynamic Characteristics and Flow Phenomena of an Unswept-Wing—Body Combination. NACA RM L52L23, 1953.
5. Pepper, William B.: The Effect on Zero-Lift Drag of an Indented Fuselage or a Thickened Wing-Root Modification to a 45° Sweptback Wing-Body Configuration As Determined by Flight Tests at Transonic Speeds. NACA RM L51F15, 1951.
6. Carmel, Melvin M.: Transonic Wind-Tunnel Investigation of the Effects of Aspect Ratio, Spanwise Variations in Section Thickness Ratio, and a Body Indentation on the Aerodynamic Characteristics of a 45° Sweptback Wing-Body Combination. NACA RM L52L26b, 1952.
7. Carmel, Melvin M.: An Experimental Transonic Investigation of a 45° Swept Wing-Body Combination With Several Types of Body Indentation With Theoretical Comparisons Included. NACA RM L54I07a, 1954.
8. Holdaway, George H.: An Experimental Investigation of Reduction in Transonic Drag Rise at Zero Lift by the Addition of Volume to the Fuselage of a Wing-Body-Tail Configuration and a Comparison With Theory. NACA RM A54F22, 1954.
9. Hall, James Rudyard: Effect on Transonic and Supersonic Drag of Fuselage Gloves Designed to Give a Smooth Overall Area Distribution to a Swept-Wing—Body Combination. NACA RM L54H30, 1954.
10. Hoffman, Sherwood: A Flight Investigation of the Transonic Area Rule for a 52.5° Sweptback Wing-Body Configuration at Mach Numbers Between 0.8 and 1.6. NACA RM L54H13a, 1954.

11. Hoffman, Sherwood: An Investigation of the Transonic Area Rule by Flight Tests of a Sweptback Wing on a Cylindrical Body With and Without Body Indentation Between Mach Numbers 0.9 and 1.8. NACA RM L53J20a, 1953.
12. Hall, James Rudyard: Comparison of Free-Flight Measurements of the Zero-Lift Drag Rise of Six Airplane Configurations and Their Equivalent Bodies of Revolution at Transonic Speeds. NACA RM L53J21a, 1954.
13. Spreiter, John R.: On the Range of Applicability of the Transonic Area Rule. NACA RM A54F28, 1954.
14. Van Driest, E. R.: Turbulent Boundary Layer in Compressible Fluids. Jour. Aero. Sci., vol. 18, no. 3, Mar. 1951, pp. 145-160, 216.
15. Morgan, Francis G., Jr., and Carmel, Melvin M.: Transonic Wind-Tunnel Investigation of the Effects of Taper Ratio, Body Indentation, Fixed Transition, and Afterbody Shape on the Aerodynamic Characteristics of a 45° Sweptback Wing-Body Combination. NACA RM L54A15, 1954.
16. Purser, Paul E.: Comparison of Wind-Tunnel, Rocket, and Flight Drag Measurements for Eight Airplane Configurations at Mach Numbers Between 0.7 and 1.6. NACA RM L54F18, 1954.
17. Henning, Allen B.: The Effect of Wing-Mounted External Stores on the Trim, Buffet, and Drag Characteristics of a Rocket-Propelled Model Having a 45° Sweptback Wing. NACA RM L54B19, 1954.

TABLE I.- FUSELAGE COORDINATES

Basic fuselage					
Nondimensional coordinates		Large fuselage, $l = 10.400$ in.		7/8-scale fuselage	
x/l	R/l	X, in.	R, in.	X, in.	R, in.
0	0	0	0	0	0
.024	.00417	.25	.0423	.219	.0370
.048	.00790	.50	.0822	.438	.0719
.072	.01152	.75	.1198	.656	.1048
.096	.01490	1.00	.1550	.875	.1356
.120	.01806	1.25	.1878	1.094	.1643
.144	.02099	1.50	.2184	1.313	.1911
.168	.02369	1.75	.2464	1.531	.2156
.192	.02617	2.00	.2722	1.750	.2382
.216	.02842	2.25	.2956	1.969	.2587
.240	.03044	2.50	.3166	2.188	.2770
.264	.03224	2.75	.3353	2.406	.2934
.288	.03381	3.00	.3516	2.625	.3077
.312	.03515	3.25	.3656	2.844	.3199
.337	.03626	3.50	.3771	3.063	.3300
.361	.03715	3.75	.3864	3.281	.3381
.385	.03781	4.00	.3932	3.500	.3441
.409	.03824	4.25	.3977	3.719	.3488
.433	.03842	4.50	.3996	3.940	.3495
.442	.03846	4.60	.4000	4.025	.3500
.456	.03846	4.75	.4000	4.150	.3500
.481	.03846	5.00	.4000	4.377	.3500
.505	.03846	5.25	.4000	4.596	.3500
.529	.03846	5.50	.4000	5.814	.3500
.553	.03846	5.75	.4000	5.032	.3500
.557	.03846	6.00	.4000	5.251	.3500
.601	.03846	6.25	.4000	5.469	.3500
.615	.03846	6.40	.4000	5.597	.3500
.625	.03846	6.50	.4000	5.688	.3500
.635	.03846	6.60	.4000	5.775	.3500
.649	.03840	6.75	.3991	5.906	.3491
.673	.03820	7.00	.3973	6.125	.3476
.697	.03769	7.25	.3920	6.344	.3439
.721	.03719	7.50	.3868	6.563	.3383
.745	.03635	7.75	.3781	6.781	.3308
.769	.03533	8.00	.3674	7.000	.3215
.793	.03412	8.25	.3549	7.219	.3105
.817	.03270	8.50	.3401	7.438	.2976
.841	.03109	8.75	.3233	7.656	.2829
.865	.02926	9.00	.3043	7.875	.2663
.889	.02726	9.25	.2835	8.094	.2481
.913	.02505	9.50	.2605	8.313	.2279
.937	.02262	9.75	.2353	8.531	.2059
.962	.01998	10.00	.2078	8.750	.1818
.986	.01720	10.25	.1789	8.969	.1565
1.000	.01538	10.40	.1600	9.100	.1400

TABLE I.- FUSELAGE COORDINATES - Continued

x/l	Fuselage radii of large winged configurations				Configurations having special wing projections	
	Fully indented fuselage and wing	Half-indented fuselage and wing	Equivalent body of fuselage and wing	Equivalent body of half-indented fuselage and wing	Root wing projection	Average wing projection
	(a)	(a)	(b)	(b)	(b)	(b)
0.481	0.3311	0.3408	0.4188	0.4095	0.4157	0.4088
.505	.3102	.3308	.4370	.4189	.4754	.4443
.529	.2892	.3210	.4538	.4279	.5149	.4723
.553	.2645	.3102	.4617	.4374	.5217	.4840
.577	.2448	.3021	.4853	.4447	.4964	.4777
.601	.2403	.3003	.4902	.4474	.4499	.4593
.615	.2419	.3009	.4909	.4479	-----	-----
.625	.2468	.3028	.4890	.4468	.4165	.4446
.649	.2631	.3092	.4780	.4405	.3995	.4337
.673	.2793	.3154	.4625	.4312	-----	.4249
.697	.2903	.3180	.4450	.4195	-----	.4195
.721	.2974	.3182	.4271	.4071	-----	.4071
.745	.3051	.3180	.4045	.3913	-----	.3913
.769	.3095	.3155	.3805	.3740	-----	.3740
.793	.3091	.3097	.3559	.3352	-----	.3352
.817	.2970	-----	.3394	.3392	-----	.3392

^a7/8-scale fuselage used.^bBasic fuselage used.

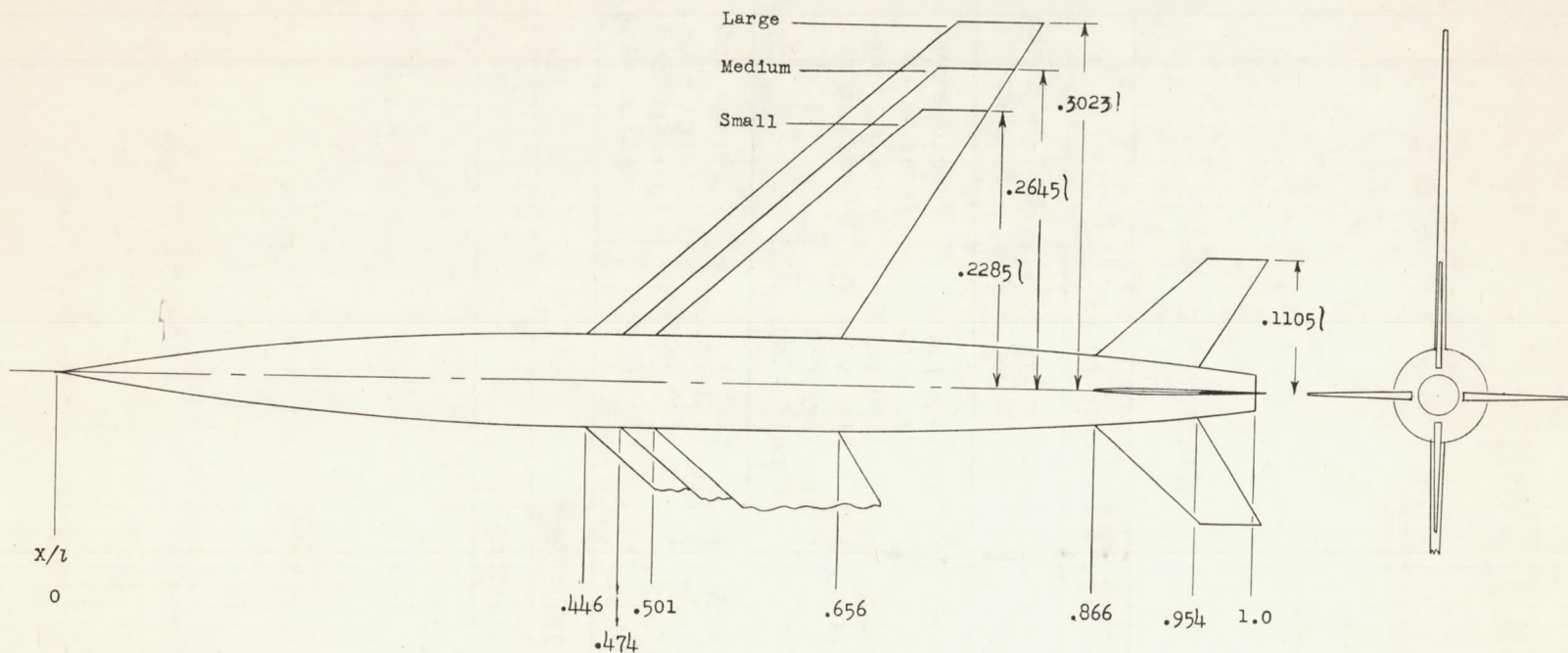
TABLE I.- FUSELAGE COORDINATES - Concluded

x/l	Fuselage radii of medium winged configurations			Fuselage radii of small winged configurations	
	Fully indented fuselage and wing (a)	Half-indented fuselage and wing (a)	Equivalent body of half-indented fuselage and wing (a)	Fully indented fuselage and wing (a)	Equivalent body of fuselage and wing (a)
0.481	0.3967	0.3985	0.4017	-----	-----
.505	.3847	.3926	.4071	0.3981	0.4021
.529	.3661	.3835	.4148	.3881	.4111
.553	.3413	.3719	.4241	.3712	.4252
.577	.3217	.3630	.4317	.3533	.4395
.601	.3111	.3583	.4361	.3394	.4503
.615	-----	-----	-----	-----	-----
.625	.3111	.3583	.4369	.3353	.4545
.635	-----	-----	-----	-----	-----
.649	.3222	.3628	.4322	.3404	.4496
.673	.3376	.3686	.4340	.3537	.4367
.697	.3473	.3707	.4133	.3608	.4218
.721	.3541	.3704	.4009	.3648	.4061
.745	.3594	.3686	.3864	.3686	.3846
.769	.3630	.3652	.3696	.3669	.3678
.793	.3545	.3545	.3545	-----	-----
.817	.3394	.3394	.3394	.3394	-----

^aBasic fuselage used.

TABLE II.- CONFIGURATIONS TESTED

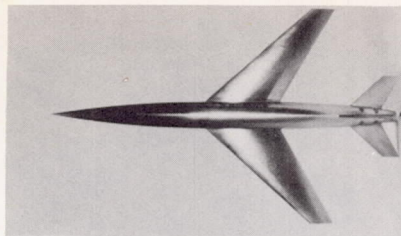
Configurations tested			
	Basic fuselage and wing	Fully indented fuselage	Half-indented fuselage
Winged configurations	Fuselage and large wing Fuselage and medium wing Fuselage and small wing	Fuselage and large wing Fuselage and medium wing Fuselage and small wing	Fuselage and large wing Fuselage and medium wing
Equivalent-body configurations	Fuselage and large wing Fuselage and small wing	(Equivalent body is the basic fuselage.)	Fuselage and large wing Fuselage and medium wing
Special wing projections	Average projection		
	Root projection		



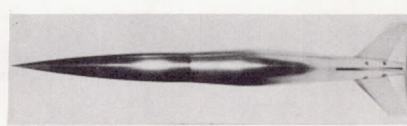
Wing geometry	Wing	Tail
NACA airfoil section	65A006	65A006
Aspect ratio	4	2.75
Taper ratio	0.3	0.49
Sweep of 1/4-chord line	45°	45°

	Wing size		
	Large	Medium	Small
Reference length . .	9.100	10.400	10.400
S_W/W_F	15.97	11.80	8.90
$\frac{S_W}{(S_F)_{\max}}$	0.490	0.360	0.277

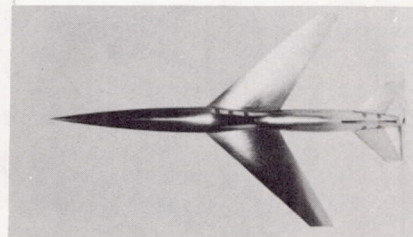
Figure 1.- Basic configurations.



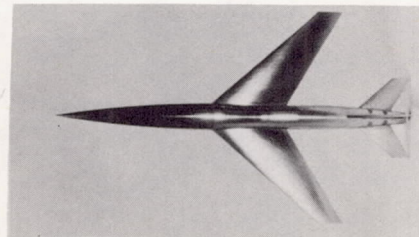
Basic large wing configuration



Equivalent body of basic large wing configuration



Large wing configuration with fuselage fully indented



Large wing configuration with fuselage half indented

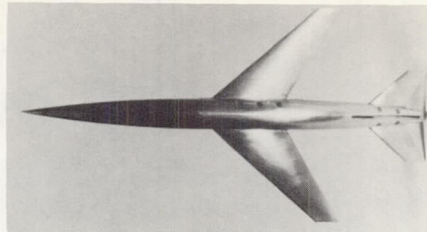


Equivalent body of large wing configuration with fuselage half indented

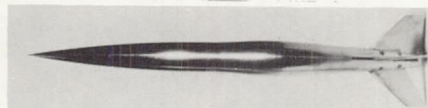
L-87969

(a) Large wing configuration and derived vehicles.

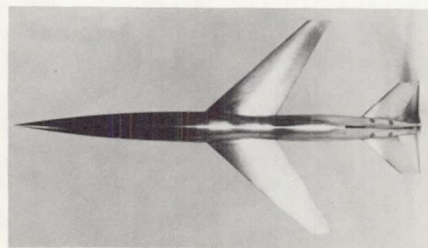
Figure 2.- Photographs of experimental vehicles.



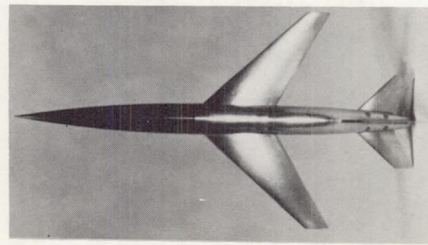
Basic medium wing configuration



Equivalent body of basic medium wing configuration (model failed)



Medium wing configuration with fuselage fully indented



Medium wing configuration with fuselage half indented

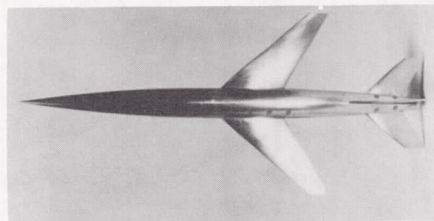


Equivalent body of medium wing configuration with fuselage half indented

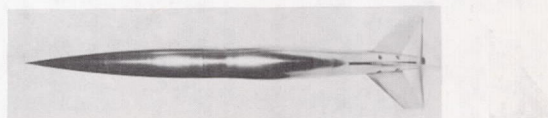
L-87970

(b) Medium wing configuration and derived vehicles.

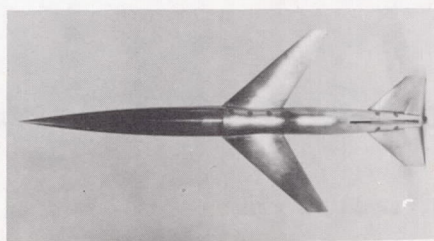
Figure 2.- Continued.



Basic small wing configuration



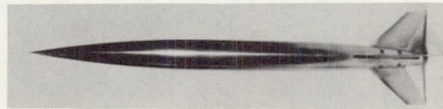
Equivalent body of small wing configuration



Small wing configuration with fully indented fuselage
L-87971

(c) Small wing configuration and derived vehicles.

Figure 2.- Continued.



Wingless vehicle



Equivalent body of medium wing configuration with the wing area taken along slices parallel to the wing maximum-thickness line (root wing projection)

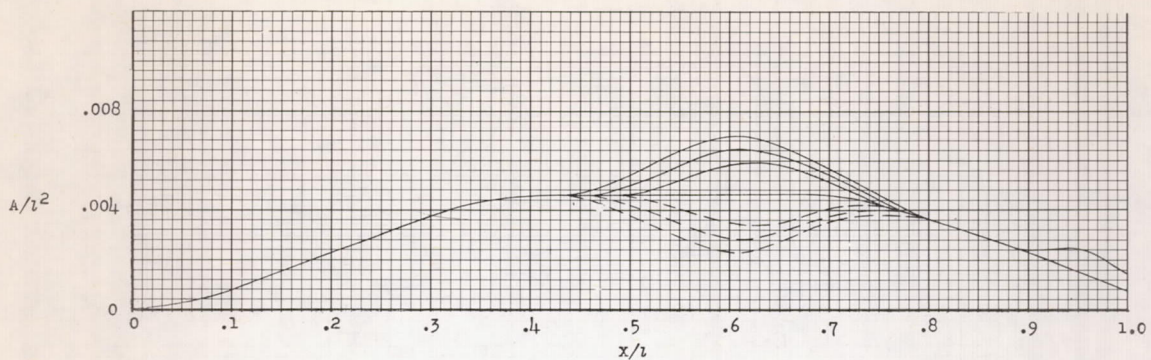


Equivalent body of medium wing configuration with the wing area taken as the average between that above and normal cross-sectional slices (average wing projection)

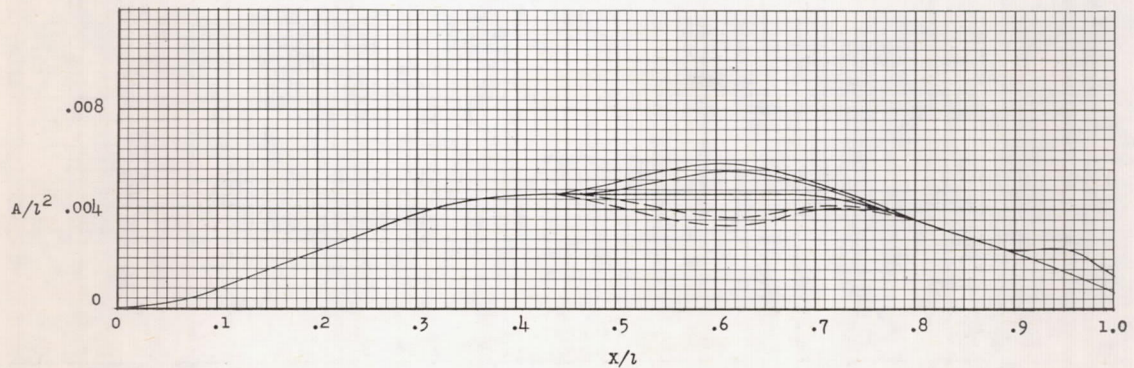
(d) Wingless vehicle and equivalent bodies with special wing projections.

L-87972

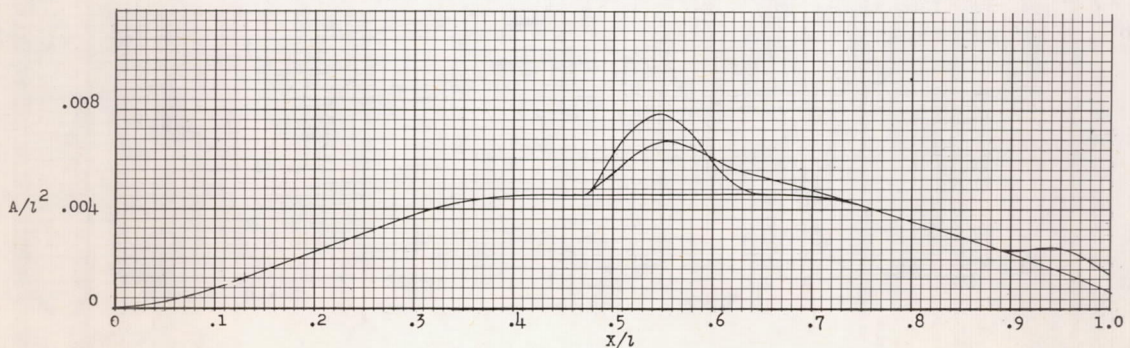
Figure 2.- Concluded.



(a) Upper curves apply to large, medium, and small wing configurations and their equivalent bodies. Center curve applies to the basic fuselage and to the three wing configurations with full indentation. The fuselage contours for the fully indented configurations are shown as broken lines.



(b) Upper curves apply to large and medium wing configurations with half indentation and to their equivalent bodies. Center line shown only for reference. Fuselage contours for half-indented configurations are shown as broken lines.



(c) Special wing projections of medium wing. Upper contour corresponds to root projection and lower contour to average projection.

Figure 3.- Nondimensional area distributions of the test vehicles.

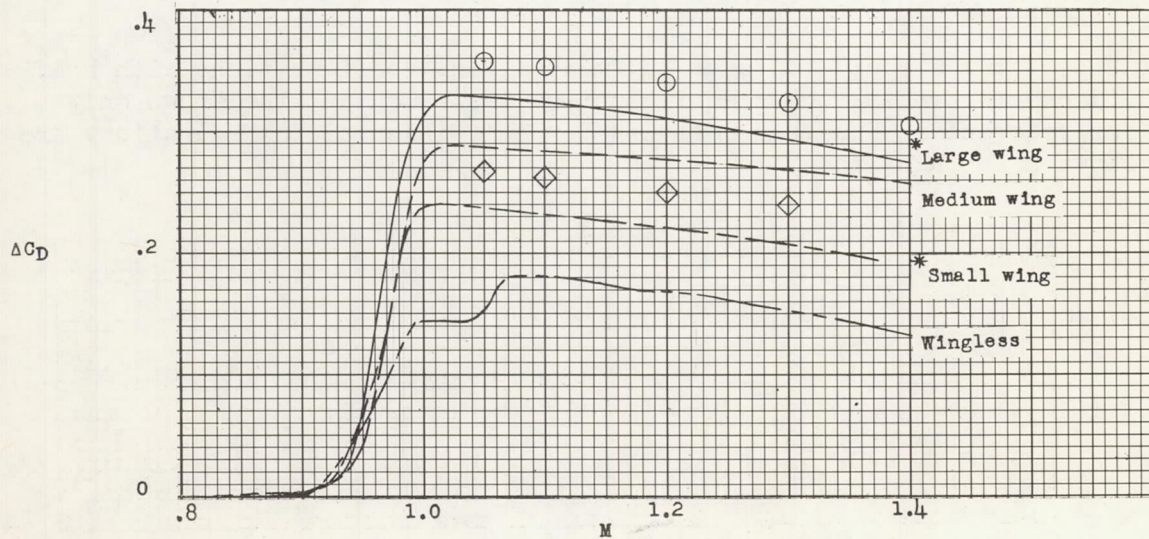
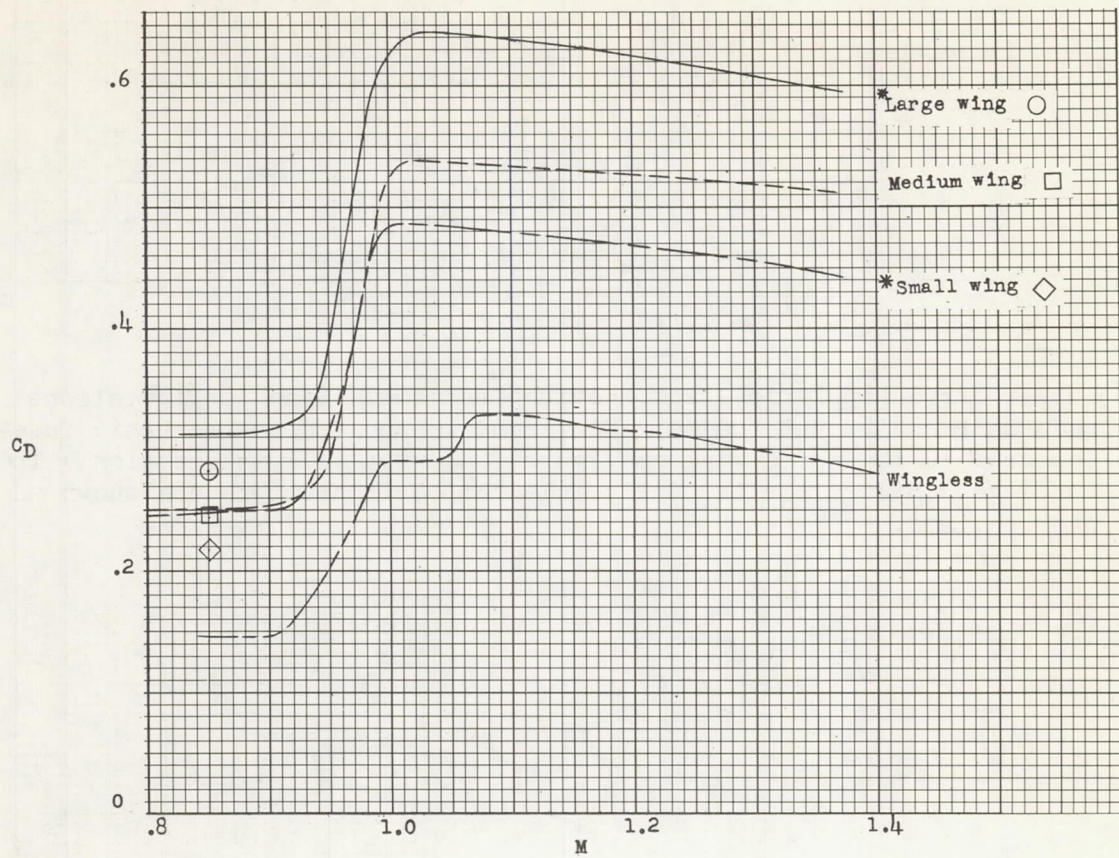


Figure 4.- Measured drag and pressure of wing configurations and wingless configurations. Curves marked with an asterisk require subsonic levels adjusted as described in the text.

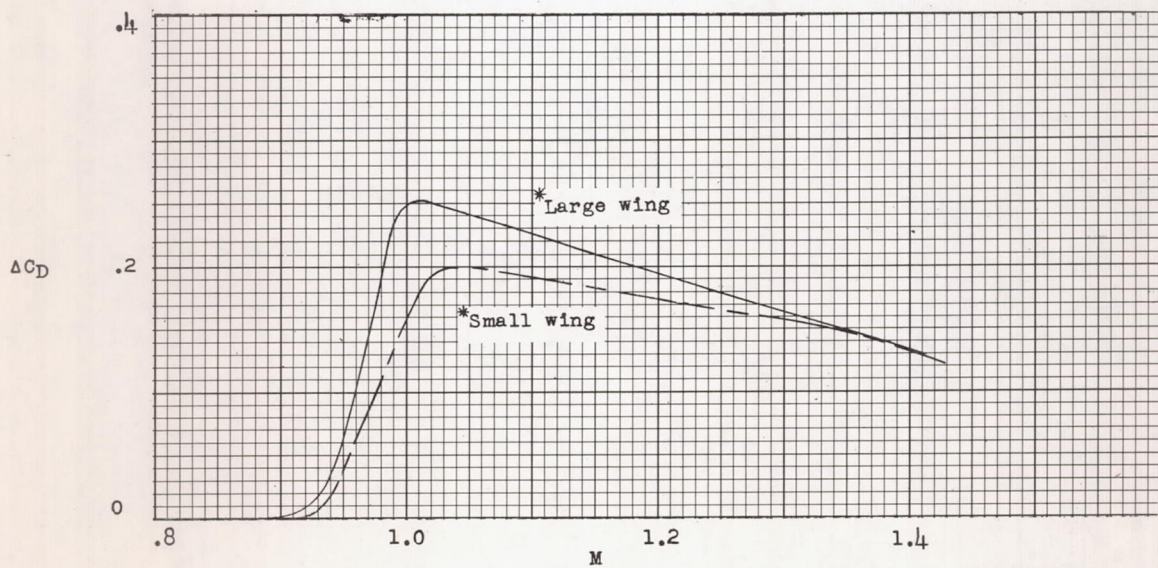
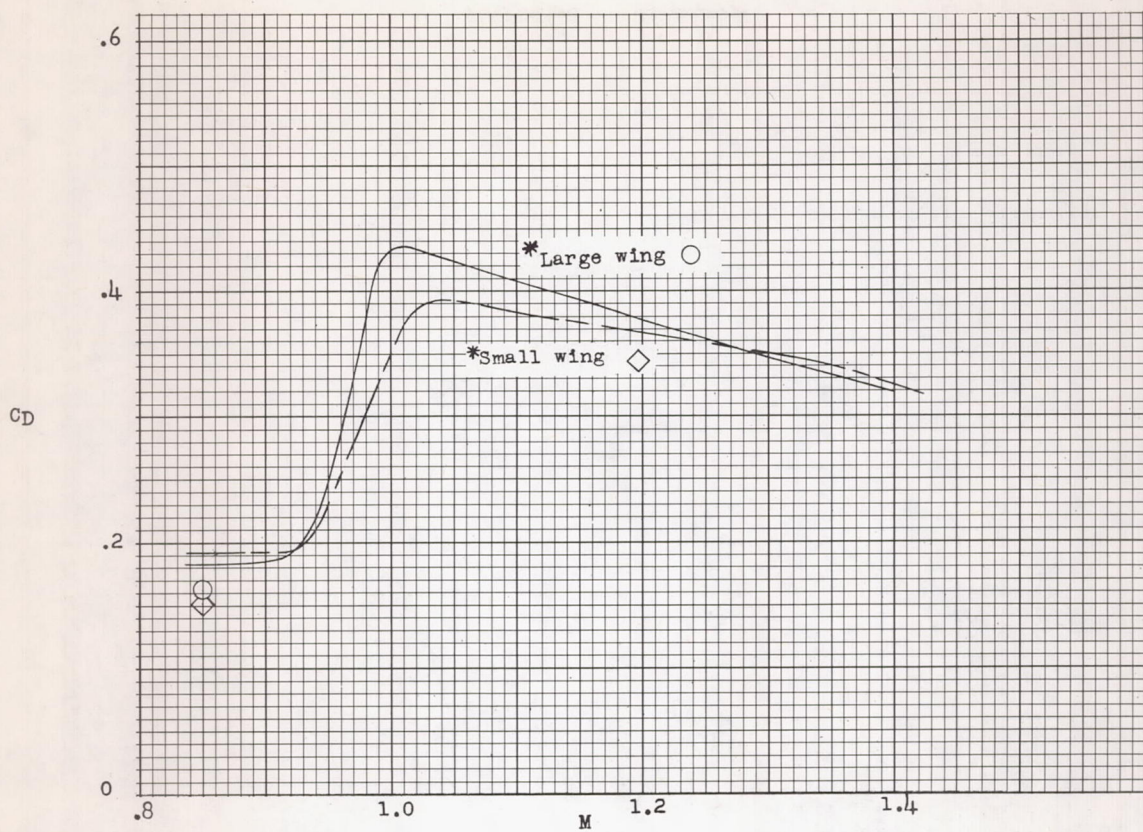


Figure 5.- Measured drag and pressure drag of equivalent bodies of wing-body configurations. Curves marked with an asterisk require subsonic level adjusted as described in the text.

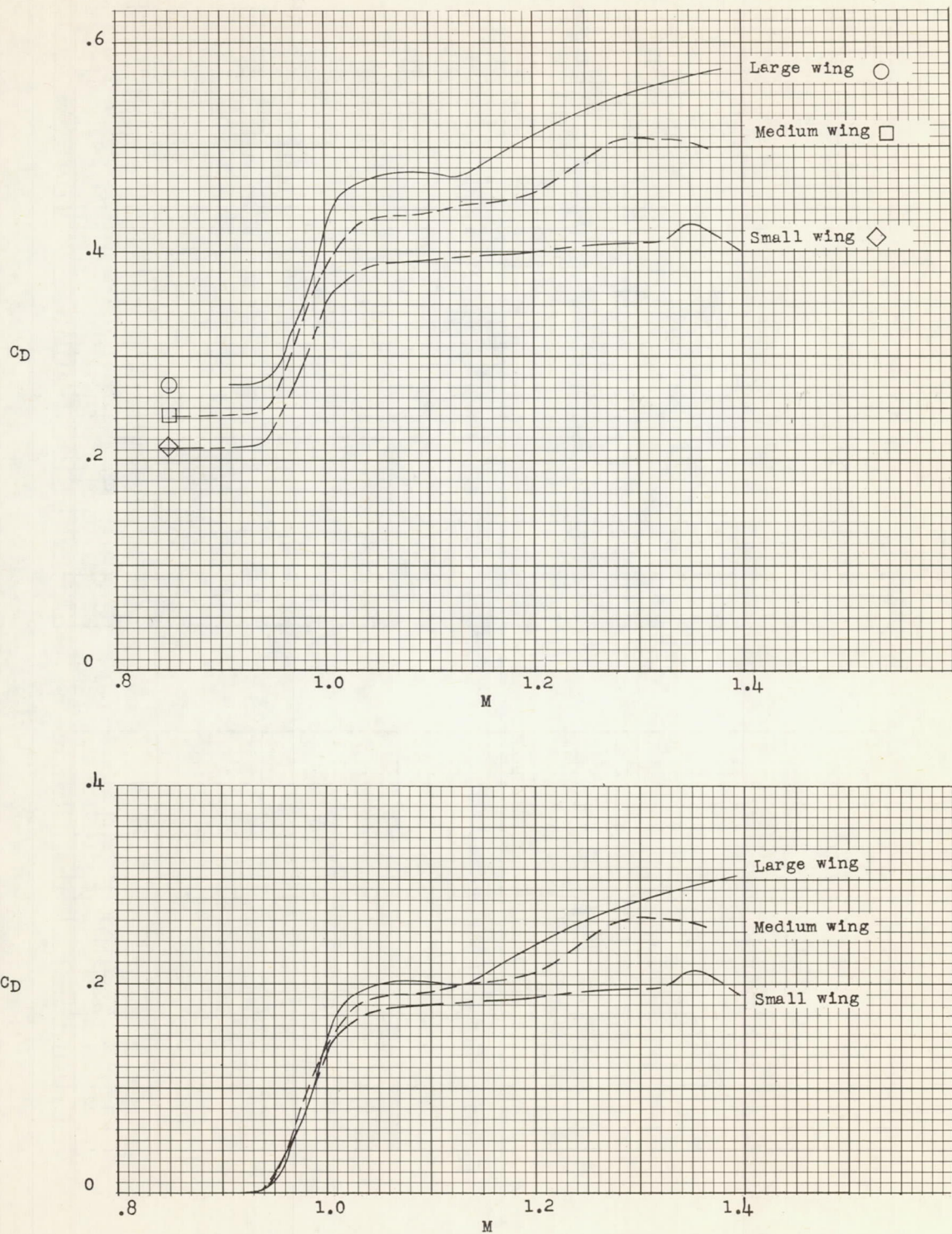


Figure 6.- Measured drag and pressure drag of fully indented wing configurations.

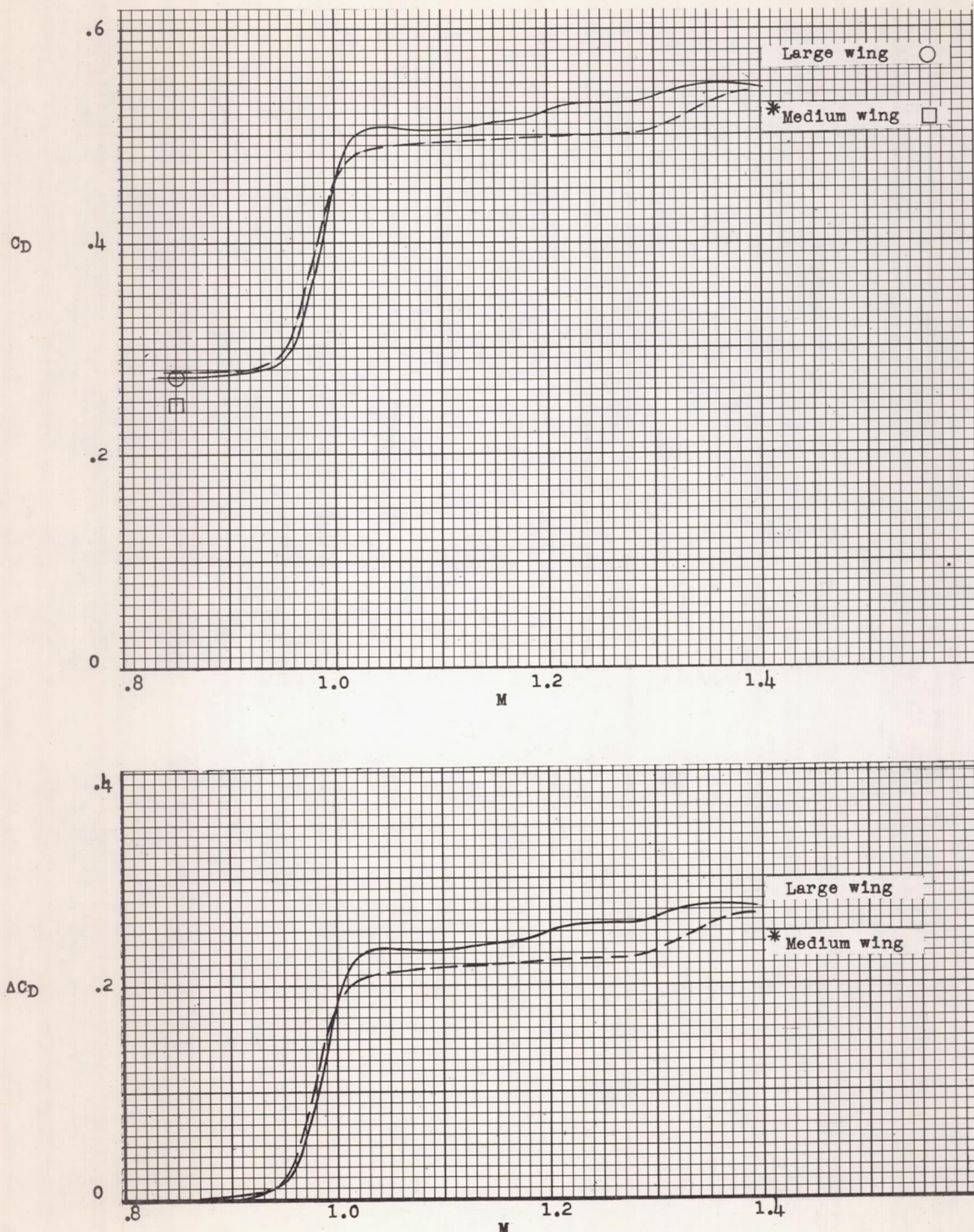


Figure 7.- Measured drag and pressure drag of half-indentation wing-body configurations. Curve marked with an asterisk requires subsonic level adjusted as described in the text.

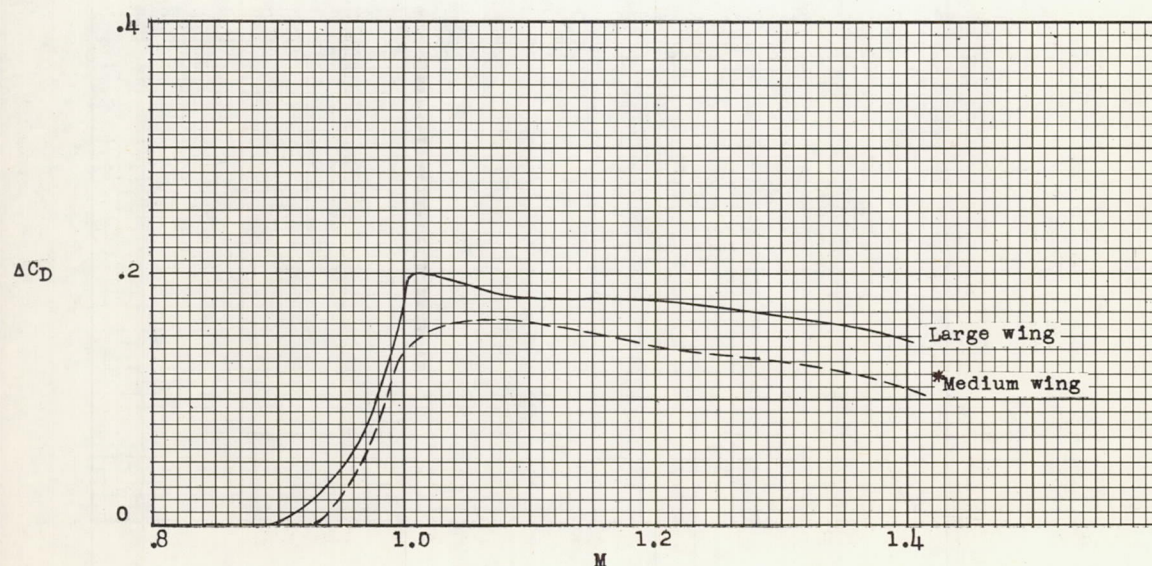
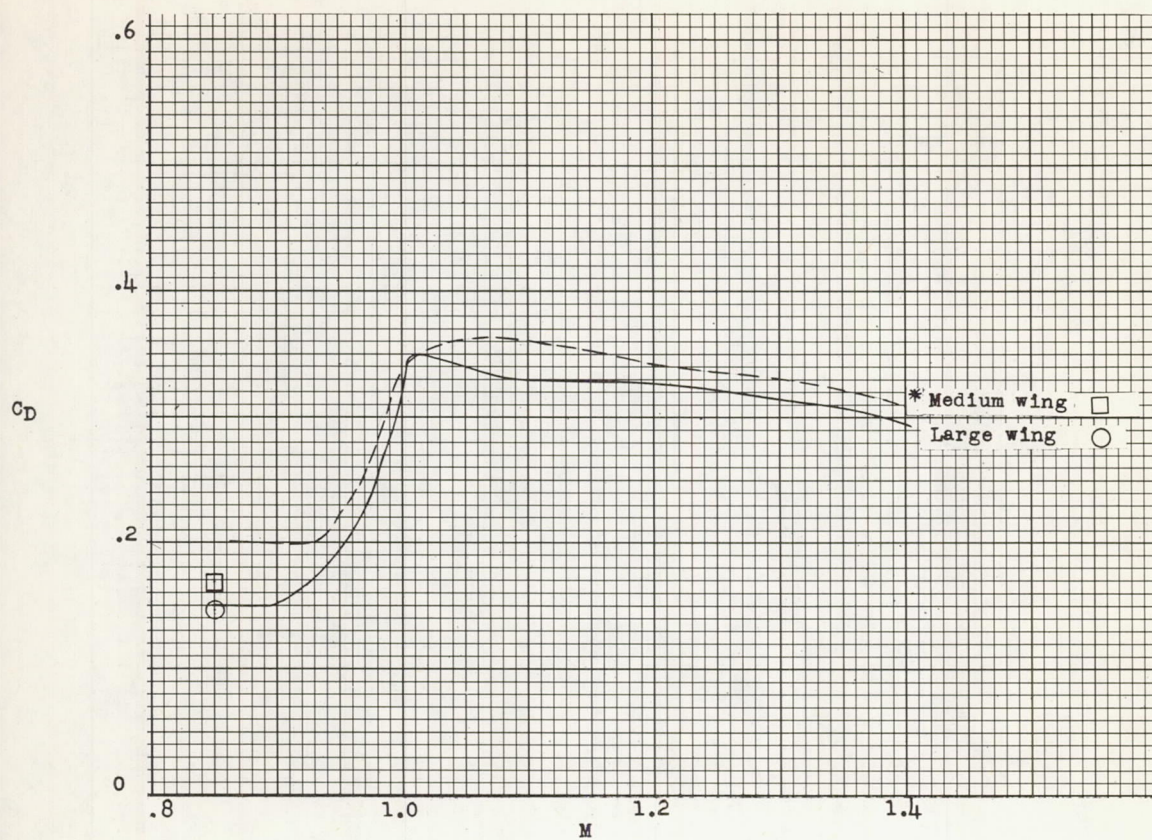


Figure 8.- Measured drag and pressure drag of equivalent bodies of half-indentured wing-body configurations. Curve marked with an asterisk requires subsonic level adjusted as described in the text.

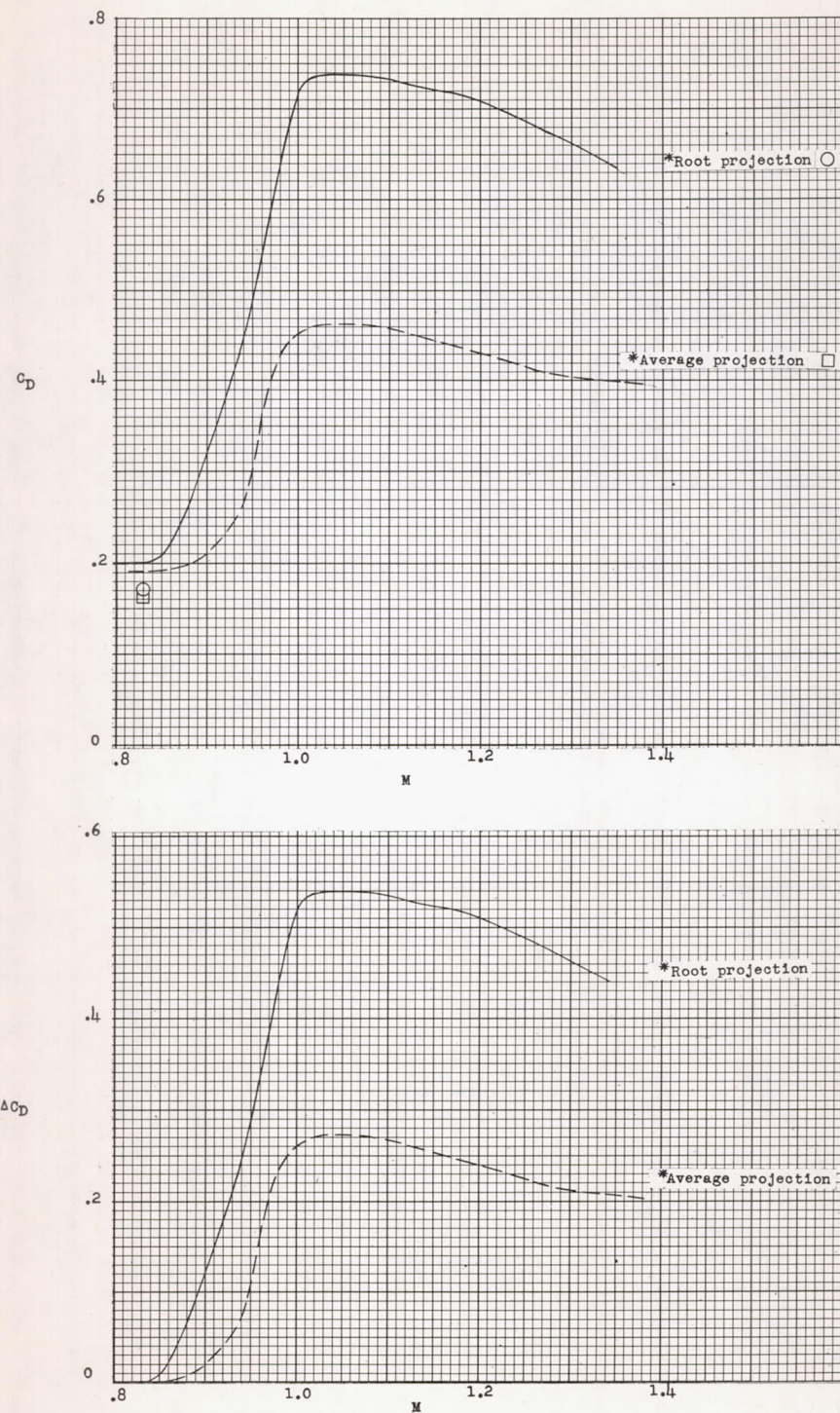


Figure 9.- Measured drag and pressure drag of two equivalent bodies of medium wing configuration incorporating special wing projections. Curves marked with an asterisk require subsonic levels adjusted as described in the text.

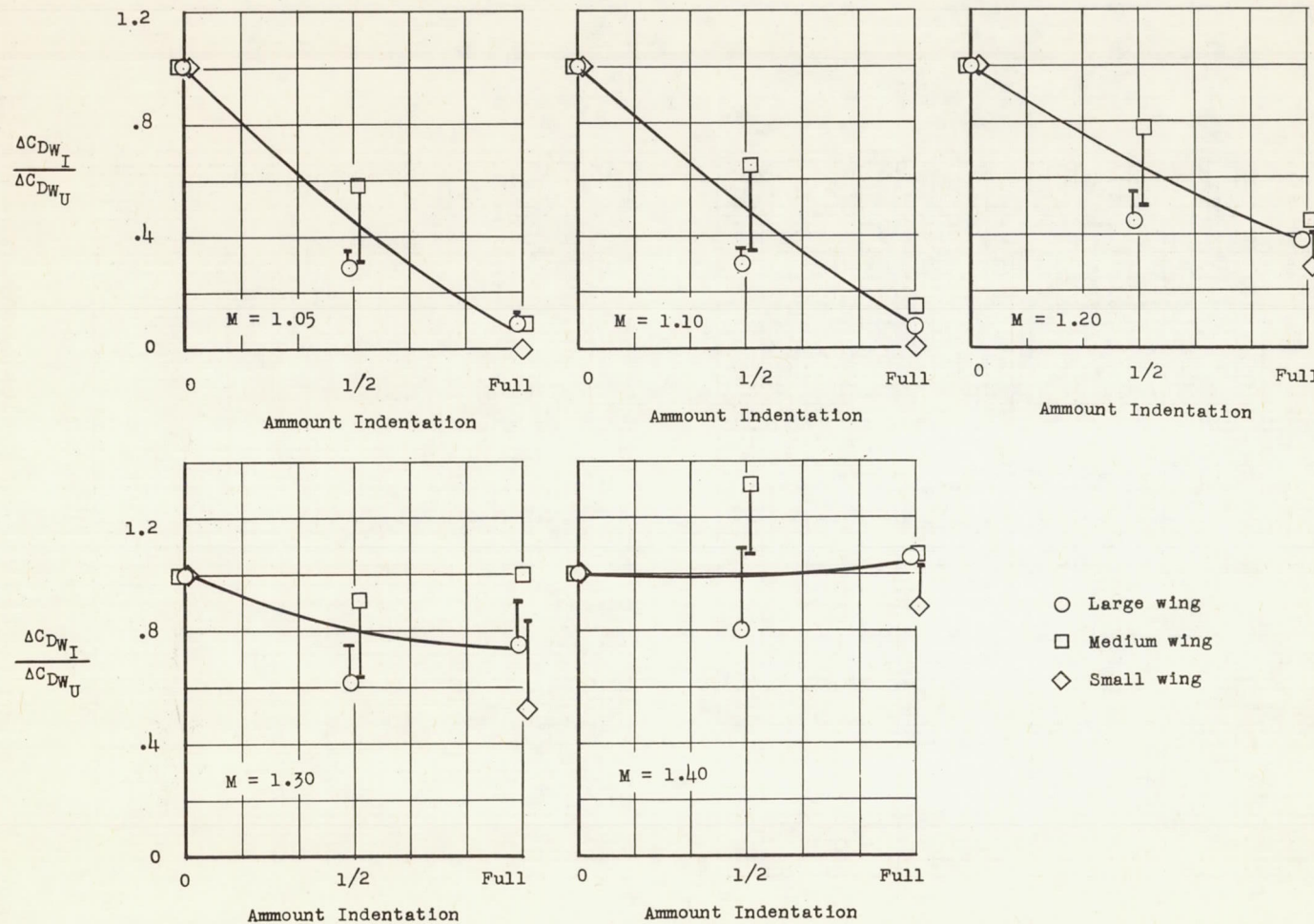
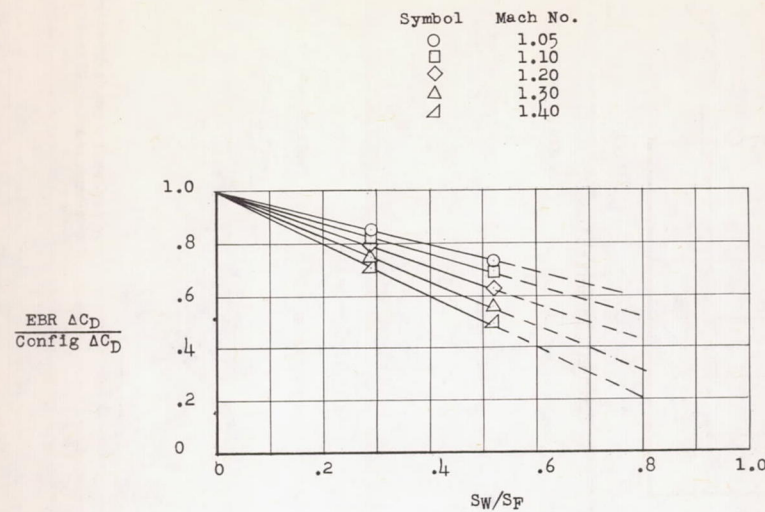
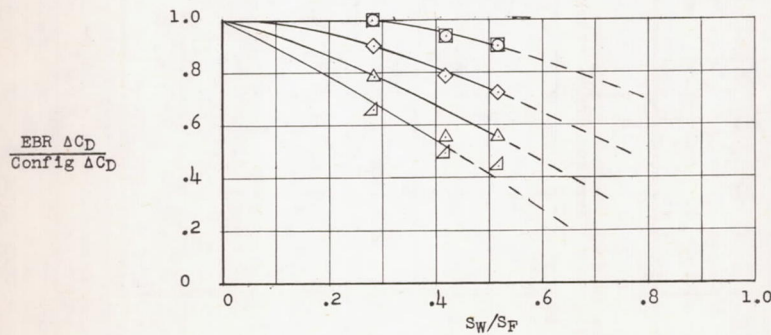


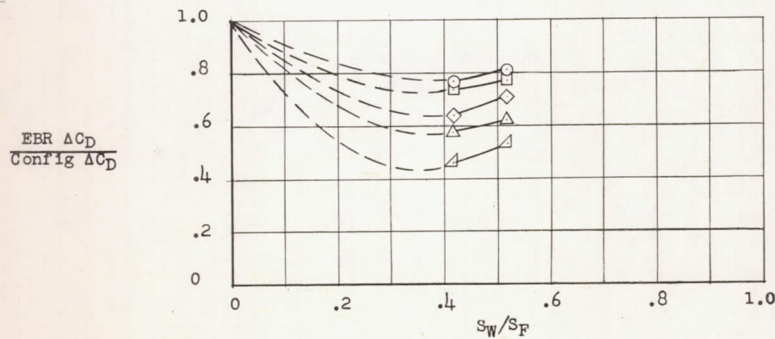
Figure 10.- Ratio of wing pressure drag with indented fuselage to wing pressure drag with unindented fuselage for three wing sizes at various Mach numbers. Results which are shown by a heavy bar connected to the symbol show the magnitude of the change which would occur had the subsonic levels not been adjusted as required.



(a) Unindented.

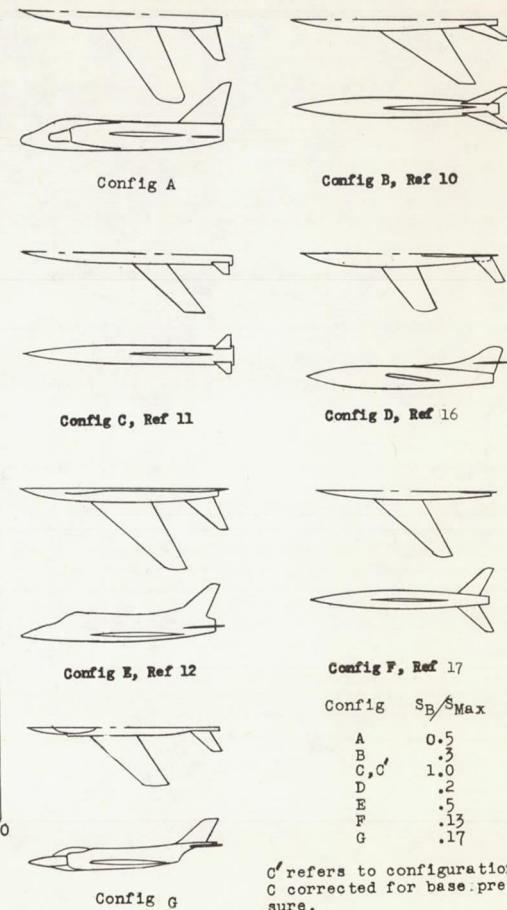
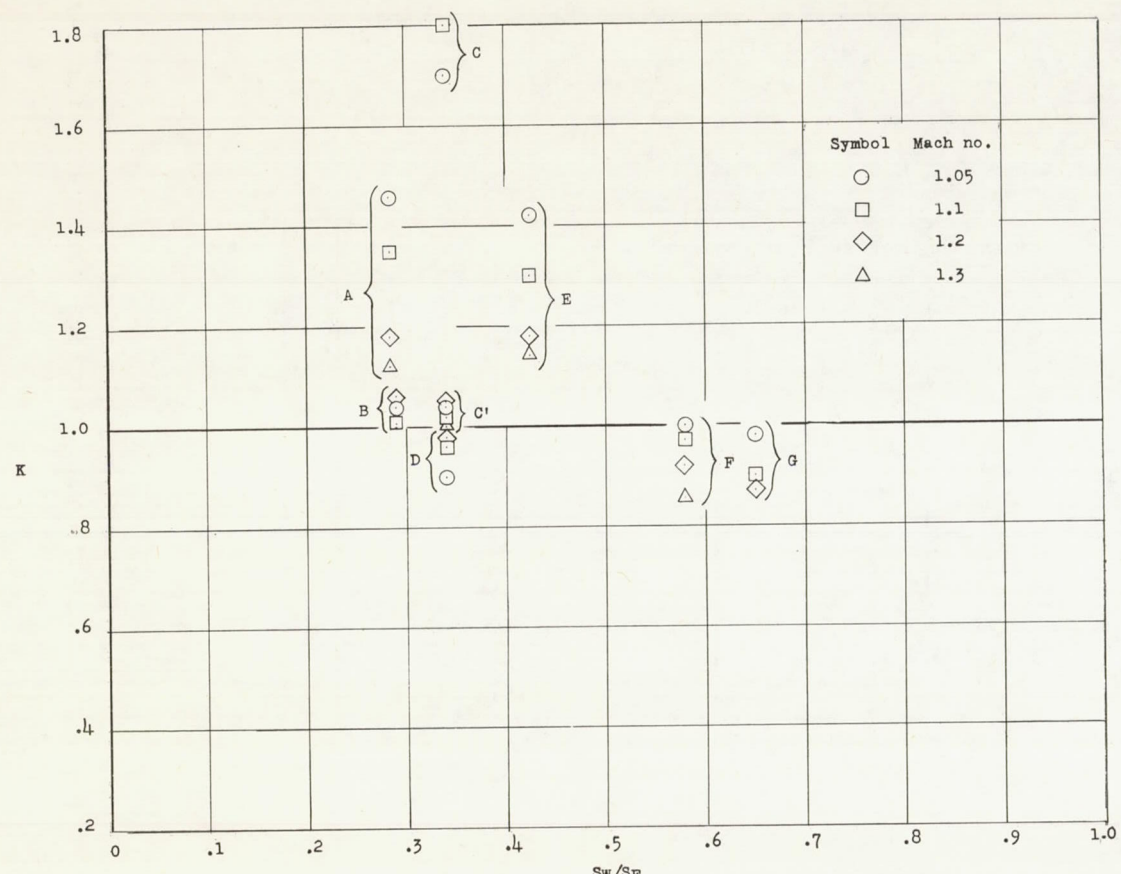


(b) Fully indented.



(c) Half indented.

Figure 11.- Variation of fraction of equivalent-body pressure drag to configuration pressure drag with wing-fuselage size ratio for various indentations.



C' refers to configuration C corrected for base pressure.

Figure 12.- Comparison of $\frac{\text{EBR } \Delta C_D}{\text{Config } \Delta C_D}$ from figure 11 with the same ratio

measured for a number of airplane configurations for appropriate wing-size ratio.

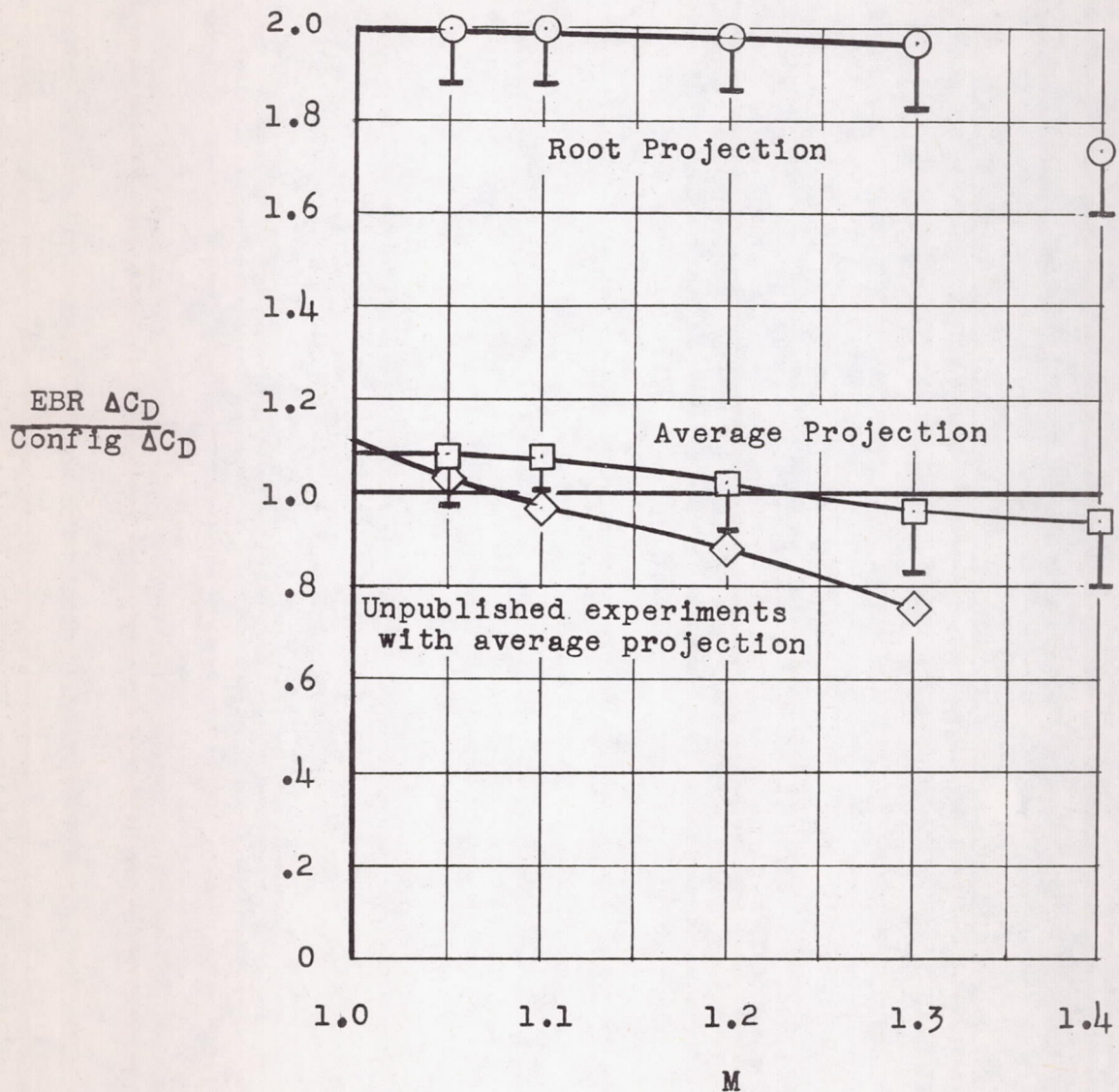


Figure 13.- Variation of $\frac{\text{EBR } \Delta C_D}{\text{Config } \Delta C_D}$ with Mach number for special wing projections. Results which are shown by a heavy bar connected to the symbol show the magnitude of the change which would occur had the subsonic levels not been adjusted as required.